



Usnic acid as potential inhibitors of BCL2 and P13K protein through network pharmacology-based analysis, molecular docking and molecular dynamic simulation

K.K.V. Wong, Miah Roney, Nazim Uddin, Syahrul Imran, Ahmad Mahfuz Gazali, Normaiza Zamri, Kamal Rullah & Mohd Fadhlizil Fasihi Mohd Aluwi

To cite this article: K.K.V. Wong, Miah Roney, Nazim Uddin, Syahrul Imran, Ahmad Mahfuz Gazali, Normaiza Zamri, Kamal Rullah & Mohd Fadhlizil Fasihi Mohd Aluwi (2023) Usnic acid as potential inhibitors of BCL2 and P13K protein through network pharmacology-based analysis, molecular docking and molecular dynamic simulation, Journal of Biomolecular Structure and Dynamics, 41:23, 13632-13645, DOI: [10.1080/07391102.2023.2178506](https://doi.org/10.1080/07391102.2023.2178506)

To link to this article: <https://doi.org/10.1080/07391102.2023.2178506>



Published online: 16 Feb 2023.



Submit your article to this journal [↗](#)



Article views: 402



View related articles [↗](#)




View Crossmark data [↗](#)



Citing articles: 6 View citing articles [↗](#)



Usnic acid as potential inhibitors of BCL2 and P13K protein through network pharmacology-based analysis, molecular docking and molecular dynamic simulation

K.K.V. Wong^{a,b}, Miah Roney^{a,b} , Nazim Uddin^c, Syahrul Imran^d, Ahmad Mahfuz Gazali^a, Normaiza Zamri^a, Kamal Rullah^e and Mohd Fadhilzil Fasihi Mohd Aluwi^{a,b}

^aFaculty of Industrial Sciences and Technology, Universiti Malaysia Pahang, Lebuhraya Tun Razak, Gambang, Pahang, Malaysia; ^bCentre for Bio-Aromatic Research, Universiti Malaysia Pahang, Lebuhraya Tun Razak, Gambang, Kuantan, Pahang Darul Makmur, Malaysia; ^cInstitute of Food Science and Technology, Bangladesh Council of Scientific and Industrial Research, Dhaka, Bangladesh; ^dAtta-ur-Rahman Institute for Natural Product Discovery, UiTM Selangor, Kampus Puncak Alam, Bandar Puncak Alam, Malaysia; ^eDrug Discovery and Synthetic Chemistry Research Group, Department of Pharmaceutical Chemistry, Kulliyah of Pharmacy, International Islamic University Malaysia, Kuantan, Pahang, Malaysia

Communicated by Ramaswamy H. Sarma

ABSTRACT

Usnic acid (UA) lately piqued the interest of researchers for its extraordinary biological characteristics, including anticancer activity. Here, the mechanism was clarified through network pharmacology, molecular docking and molecular dynamic simulation. Sixteen proteins were selected through network pharmacology study as they are probable to interact with UA. Out of these proteins, 13 were filtered from PPI network analysis based on their significance of interactions ($p < 0.05$). KEGG pathway analysis has also aided us in determining the three most significant protein targets for UA, which are BCL2, PI3KCA and PI3KCG. Therefore molecular docking and molecular dynamic (MD) simulations throughout 100 ns were performed for usnic acid onto the three proteins mentioned. However, UA's docking score in all proteins is lower than their co-crystallised ligand, especially for BCL2 (−36.5158 kcal/mol) and PI3KCA (−44.5995 kcal/mol) proteins. The only exception is PI3KCG which has comparable results with the co-crystallised ligand with (−41.9351 kcal/mol). Furthermore, MD simulation has also revealed that usnic acid does not stay fit in the protein throughout the simulation trajectory for PI3KCA protein evident from RMSF and RMSD plots. Nevertheless, it still poses good ability in inhibiting BCL2 and PI3KCG protein in MD simulation. In the end, usnic acid has exhibited good potential in the inhibition of PI3KCG proteins, rather than the other proteins mentioned. Thus further study on structural modification of usnic acid could enhance the ability of usnic acid in the inhibition of PI3KCG as anti-colorectal and anti-small cell lung cancer drug candidate.

ARTICLE HISTORY

Received 25 July 2022
Accepted 3 February 2023

KEYWORDS

MD simulation; network pharmacology; PPI; molecular docking; usnic acid

1. Introduction

Cancer is a disease where cells in the body grow uncontrollably and spread to other parts of the body (NIH, 2021). It has been the leading cause of death worldwide and nausea (WHO, 2020). Although cancer treatments such as commonly used radiotherapy and chemotherapy (ACS, 2022) have been implemented for ages, yet the situation of cancer being a world-leading cause of death persists. Better cancer treatment is often related to expensive costs, and it is unbearable for the majority of society. Thus, discoveries of small molecules for cancer treatment (chemotherapy) have always been a struggle to invent more cost-effective drugs that the majority of the population could afford.

With the complement of this effort, new technologies had to come into action to aid drug discoveries. Network pharmacology is a modern tool that could understand the complex interaction between ligands with multiple targets (Hopkins, 2007). A paradigm shift from "one drug, one

target" to "multicomponent therapeutics/biological complexes" is the main goal of the network pharmacology method (Belenahalli Shekarappa et al., 2019). This involves researching the various ways that medications can affect different tissues and cell types as well as the various ways that different crosstalk pathways can lead to varied activities within a single cell type (Liu et al., 2009). Different approaches can be used to illustrate how biological processes operate in the body. With network pharmacology, one could disclose the underlying relationship between natural products and cancers. Thus, finding the most suitable target for the selected chemical compound is possible.

The collection of genes and proteins that interact with one another to produce biological processes, molecular functions, and cellular components are known as protein-protein interaction complexes (PPI) or signalling pathways. When pathways that convey signals from one gene to another are activated or repressed, proteins and genes are represented as nodes in the KEGG (Kyoto Encyclopaedia of Genes and

Genomes) signalling pathways and signals and connections are represented as edges (Belenahalli Shekarappa et al., 2019). Identification of hub nodes in large-scale free PPI networks depends critically on in silico biological network validation and analysis. In a complex biological system, the hub nodes are highly interconnected functional proteins that sustain the global network and cell-cell communication. These nodes are related to one another through physical interactions (Paris & Bazzoni, 2008).

With the reasoning mentioned above, thus, selected usnic acid (UA) as our natural target product in this case. UA is a secondary metabolite from the lichen *Usnea florida*. *Usnea* is the most commonly used genus of lichens for traditional medicine (Crawford, 2015). It has been used in various daily products such as deodorant and toothpaste (Prateeksha et al., 2016). Other than that, it has been initially used to treat sore throats, colds, and bacterial infections (Prateeksha et al., 2016). In recent years, researchers discovered that UA poses a variety of bioactivities, such as anti-bacterial activity by targeting *Mycobacterium tuberculosis* (Bangalore et al., 2020), antiviral activity by targeting Hepatitis C virus (Wei et al., 2020), and its potential anticancer properties with targeting leukaemia, breast and prostate cancer (Nguyen et al., 2021){Ebrahim, 2017 #57}. Currently, scientists are interested in researching potential anticancer inhibitory signalling pathways of UA. For instance, it has been found that UA blocks the Akt/mTOR signalling pathway, {Eryilmaz, 2018 #56} however, there is no studies have been reported on others possible signalling pathways. Therefore, it is crucial to investigate other signalling pathways that may serve as targets for the treatment of cancers (Chen et al., 2014; Kwong & Wang, 2020).

On the other hand, molecular docking simulations and molecular dynamic (MD) simulations are two of the prediction tools that could be utilised to predict the interaction between proteins and ligands. Molecular docking simulations could be used to simulate the interaction between the proposed ligand with the targeted proteins. By doing the simulations, the prediction of interaction energy could be obtained and used to predict the efficiency of the proposed ligand (Hussein & Elkhair, 2021). While MD simulation provides the ability to simulate ligand-protein complex in a non-rigid condition and provide water molecules as surrounding to simulate the situation in the human body further (Singh et al., 2018).

To investigate the pharmacological mechanisms of UA as a therapy for anti-colorectal and anti-small cell lung cancer, we used a network pharmacology approach in this study. In order to determine the probable mechanism of action of UA against colorectal and small cell lung cancer, protein-protein interaction (PPI) data were first gathered from the STRING database. Additionally, MD simulations of the best complexes were run against the selected proteins (BCL2, PI3KCA, and PI3KCG). Overexpression of the well-known pro-survival protein and critical apoptosis regulators are both regulated by proteins in BCL2. BCL2 is a characteristic that is frequently found in human adenocarcinomas and is responsible for the dysregulation of apoptosis, which renders tumour cells

resistant to traditional cancer therapy drugs and prevents the death of cancer cells (Leibowitz & Yu, 2010). Additionally, increased anti-apoptotic Bcl-2 protein expression promotes tumorigenesis as well as the ability of MCF-7 breast cancer cells to migrate, invade, and spread (Kamath et al., 2016). Additionally, increased VEGF expression brought on by BCL2 overexpression boosts neo-angiogenesis in human cancer xenografts (Liu et al., 2019). Additionally, PI3Ks (PI3KCA and PI3KCG) control a number of significant cellular functions through this phosphorylation, including growth, proliferation, and survival (Asati et al., 2016). Therefore, it appears that BCL2, PI3KCA, and PI3KCG are important chemotherapeutic targets for the treatment of breast cancer. In conclusion, our study used network pharmacology, docking, and MD simulation to discover possible targets and pathways of UA as a treatment against colorectal and small-cell lung cancer.

2. Results and discussions

2.1. UA interacting with target proteins

It is essential for understanding the target proteins on which UA acts. It was found that UA significantly (Interaction probability ≥ 0.10) interacted with 16 target proteins (PTGES (Prostaglandin E synthase), ALOX5 (Arachidonate 5-lipoxygenase), PDE5A (Phosphodiesterase 5 A), EGLN1 (Egl-9 Family Hypoxia Inducible Factor 1), HSP90AB1 (Heat shock protein HSP 90-beta gene), HSP90B1 (Heat Shock Protein 90 Beta Family Member 1), HSP90AA1 (Heat shock protein HSP 90-alpha gene), CBR1 (Carbonyl reductase 1), MTOR (Mammalian Target of Rapamycin), PIK3CG (Phosphatidylinositol-4,5-bisphosphate 3-kinase catalytic subunit gamma isoform), PIK3CA (Phosphatidylinositol-4,5-bisphosphate 3-kinase catalytic subunit alpha isoform), CXCR2 (CXC chemokine receptor 2), PRKAA1 (Protein Kinase AMP-Activated Catalytic Subunit Alpha 1), NPY5R (Neuropeptide Y Receptor Y5), PPARG (Peroxisome proliferator-activated receptor gamma), and BCL2 (B-cell lymphoma 2)). The target proteins' interactions with UA in was depicted in Figure 1. Cytoscape 3.8.2 was used to analyse the interaction between UA and all target proteins (probability ≥ 0.10). Based on the UA-protein targets relationships, it is now clear that UA is having interaction with the target proteins. These results indicate that UA plays substantial biological and physiological activities.

2.2. Target proteins are associated with protein-protein interaction (PPI) network

PPI network plays substantial roles in molecular processes, and abnormal PPI is the basis of many pathological conditions (Wong et al., 2009). Using STRING (Szkarczyk et al., 2019) database, all target proteins (16) were mapped into the PPI network. Interestingly, 13 target proteins are involved in PPI, which have 25 edges, and an average node degree of 3.12 with the PPI enrichment p-value is 7.67×10^{-07} . In this PPI network, the larger the node degree, the stronger the relationship between the proteins corresponding to the node in this network, which indicates that the target proteins play a key role in the whole interaction network, the

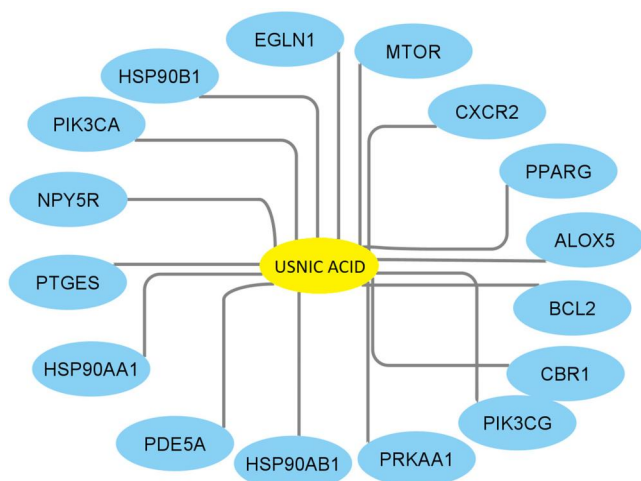


Figure 1. UA-target protein interaction network. The yellow node represents the UA, and the blue nodes represent the 16 target proteins.

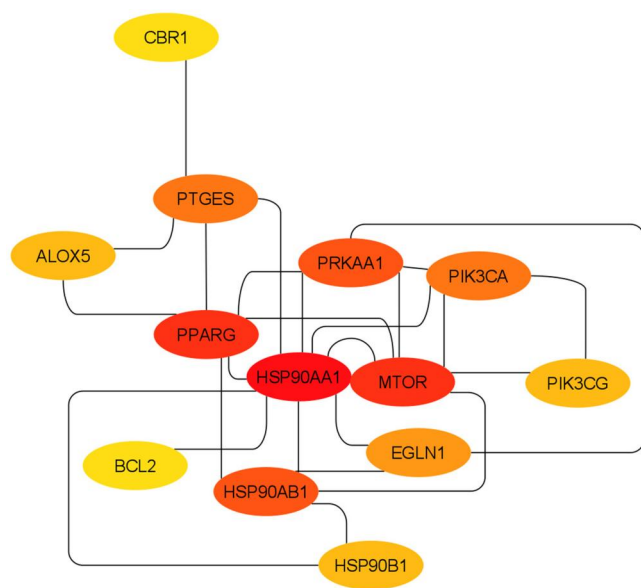


Figure 2. Protein-protein interaction (PPI) network of 13 interacted target proteins.

important target protein. Only PDE5A, CXCR2, and NPY5R proteins are not included in PPI.

Top-ranked target proteins with the best degree of interaction with other proteins are illustrated in Figure 2. Cytoscape 3.8.2 was used to analyse the interaction among target proteins. Figure 2 shows that most of the HSP90AA1, PPARG, MTOR, PRKAA1 and HSP90AB1 are centrally located in the PPI networks with the best degree of interaction, indicating that this PPI network is associated with biological activities.

2.3. Target protein sets that are associated with the enrichment of KEGG pathways

To further elucidate the relationship between target proteins and the pathways, 21 KEGG pathways that were significantly (False discovery rate (FDR) ≤ 0.05) associated with the target proteins (Table 1) were identified. These pathways were mainly involved in cancer (Prostate cancer, Pathways in cancer, Acute

myeloid leukaemia, Colorectal cancer, Central carbon metabolism in cancer, Glioma, Renal cell carcinoma, and small cell lung cancer) and cellular signalling (PI3K-Akt signalling pathway, Hypoxia-Inducible Factor (HIF-1) signalling pathway, Estrogen (ER) signalling pathway, Adenosine Monophosphate-Activated Protein Kinase (AMPK) signalling pathway, mTOR signalling pathway, Progesterone-mediated oocyte maturation, Insulin signalling pathway, and Erythroblastic Leukemia Viral Oncogene Homologue (ErbB) signalling pathway). Interestingly PIK3CA, BCL2, and PIK3CG genes are associated with the colorectal cancer pathway (Figure 3) and small cell lung cancer pathway (Figure 4). Altogether, it indicates that UA may control the cancerous pathways by inhibiting PPI networks.

BCL2 proteins are the key regulators of cell death, which induce cell death by apoptosis and have been the target for a wide range of cancers (Huang, 2000). The inhibition of BCL2 can serve as the main ingredient of neutralizing the effect of these anti-apoptotic proteins, which will lead to the control of cancer cells (Vogler et al., 2009). Whereas PI3K is one of the upstream proteins that coordinate the intracellular signalling who reacts to surrounding stimulators (Noorolyai et al., 2019). Since PI3K protein is upstream of cell survivor signalling pathways, inhibiting this protein simply is effective to eliminate the target cancer cells.

2.4. Molecular docking

Consistent with the results from network pharmacology, further investigation and validation of these results have been performed with the molecular docking simulation method. The simulation is a step to validate the effectiveness of UA in the inhibition of BCL2 and PI3K proteins.

After moving on to the verification of the ability of UA using molecular docking, it was found that UA can inhibit the three proteins that have been deduced from our network pharmacology study. UA can form at least two hydrogen bonds with the target protein. At the same time, it is proven that hydrogen bonding is the essential key for the inhibition that occurs in proteins (Kostal, 2016), showing that UA poses the ability in inhibiting the three target proteins in the study.

Based on the molecular docking simulation results, UA had taken on an expanded shape that fit precisely into the binding pockets of the target protein was observed (Figure 5a). Two hydroxyl hydrogen of benzene ring projected two hydrogen bonds with the residues of Asn B:169 and Trp B:173 in the distance of 2.40 Å and 2.17 Å, respectively. Other than that, two carbonyl groups from UA also mediated two hydrogen bonds with the residues of Arg B:124 and Trp A;173 in the distance of 2.00 Å and 2.10 Å, respectively. The methyl group of UA formed two alkyl/pi-alkyl interactions with the residues of Leu B:172 and Trp B:173. Our study revealed that the binding affinity of UA and the target protein is -36.5158 kcal/mol (Table 2), which is much lower than the co-crystallised ligand. Thus, structural modification of UA should be the priority before making it a valuable drug candidate targeting the inhibitory effect of BCL2 protein.

On the other hand, the co-crystallised ligand (Pubchem CID:71656179) had a binding affinity of -73.5126 kcal/mol

Table 1. Enriched KEGG pathways that are significantly associated with target proteins of UA.

KEGG PATHWAY	Count	p-value	Genes	FDR value
hsa05215:Prostate cancer	7	1.68E-08	HSP90AA1, HSP90AB1, PIK3CA, BCL2, MTOR, PIK3CG, HSP90B1	1.25E-06
hsa05200:Pathways in cancer	9	4.78E-07	EGLN1, HSP90AA1, HSP90AB1, PIK3CA, BCL2, PPARG, MTOR, PIK3CG, HSP90B1	1.77E-05
hsa04151:PI3K-Akt signalling pathway	8	3.41E-06	HSP90AA1, PRKAA1, HSP90AB1, PIK3CA, BCL2, MTOR, PIK3CG, HSP90B1	8.41E-05
hsa04066:HIF-1 signalling pathway	5	4.32E-05	EGLN1, PIK3CA, BCL2, MTOR, PIK3CG	7.22E-04
hsa04915:Estrogen signalling pathway	5	4.88E-05	HSP90AA1, HSP90AB1, PIK3CA, PIK3CG, HSP90B1	7.22E-04
hsa04152:AMPK signalling pathway	5	1.14E-04	PRKAA1, PIK3CA, PPARG, MTOR, PIK3CG	1.41E-03
hsa04150:mTOR signalling pathway	4	2.41E-04	PRKAA1, PIK3CA, MTOR, PIK3CG	2.55E-03
hsa04914:Progesterone-mediated oocyte maturation	4	7.97E-04	HSP90AA1, HSP90AB1, PIK3CA, PIK3CG	7.37E-03
hsa04931:Insulin resistance	4	1.49E-03	PRKAA1, PIK3CA, MTOR, PIK3CG	1.23E-02
hsa04910:Insulin signalling pathway	4	3.01E-03	PRKAA1, PIK3CA, MTOR, PIK3CG	2.23E-02
hsa04930:Type II diabetes mellitus	3	4.72E-03	PIK3CA, MTOR, PIK3CG	3.18E-02
hsa04141:Protein processing in endoplasmic reticulum	4	5.33E-03	HSP90AA1, HSP90AB1, BCL2, HSP90B1	3.29E-02
hsa05221:Acute myeloid leukaemia	3	6.39E-03	PIK3CA, MTOR, PIK3CG	3.42E-02
hsa00590:Arachidonic acid metabolism	3	7.54E-03	CBR1, ALOX5, PTGES	3.42E-02
hsa05210:Colorectal cancer	3	7.78E-03	PIK3CA, BCL2, PIK3CG	3.42E-02
hsa04210:Apoptosis	3	7.78E-03	PIK3CA, BCL2, PIK3CG	3.42E-02
hsa05230:Central carbon metabolism in cancer	3	8.28E-03	PIK3CA, MTOR, PIK3CG	3.42E-02
hsa05214:Glioma	3	8.53E-03	PIK3CA, MTOR, PIK3CG	3.42E-02
hsa05211:Renal cell carcinoma	3	8.78E-03	EGLN1, PIK3CA, PIK3CG	3.42E-02
hsa05222:Small cell lung cancer	3	1.43E-02	PIK3CA, BCL2, PIK3CG	5.0E-02
hsa04012:ErbB signalling pathway	3	1.49E-02	PIK3CA, MTOR, PIK3CG	5.0E-02

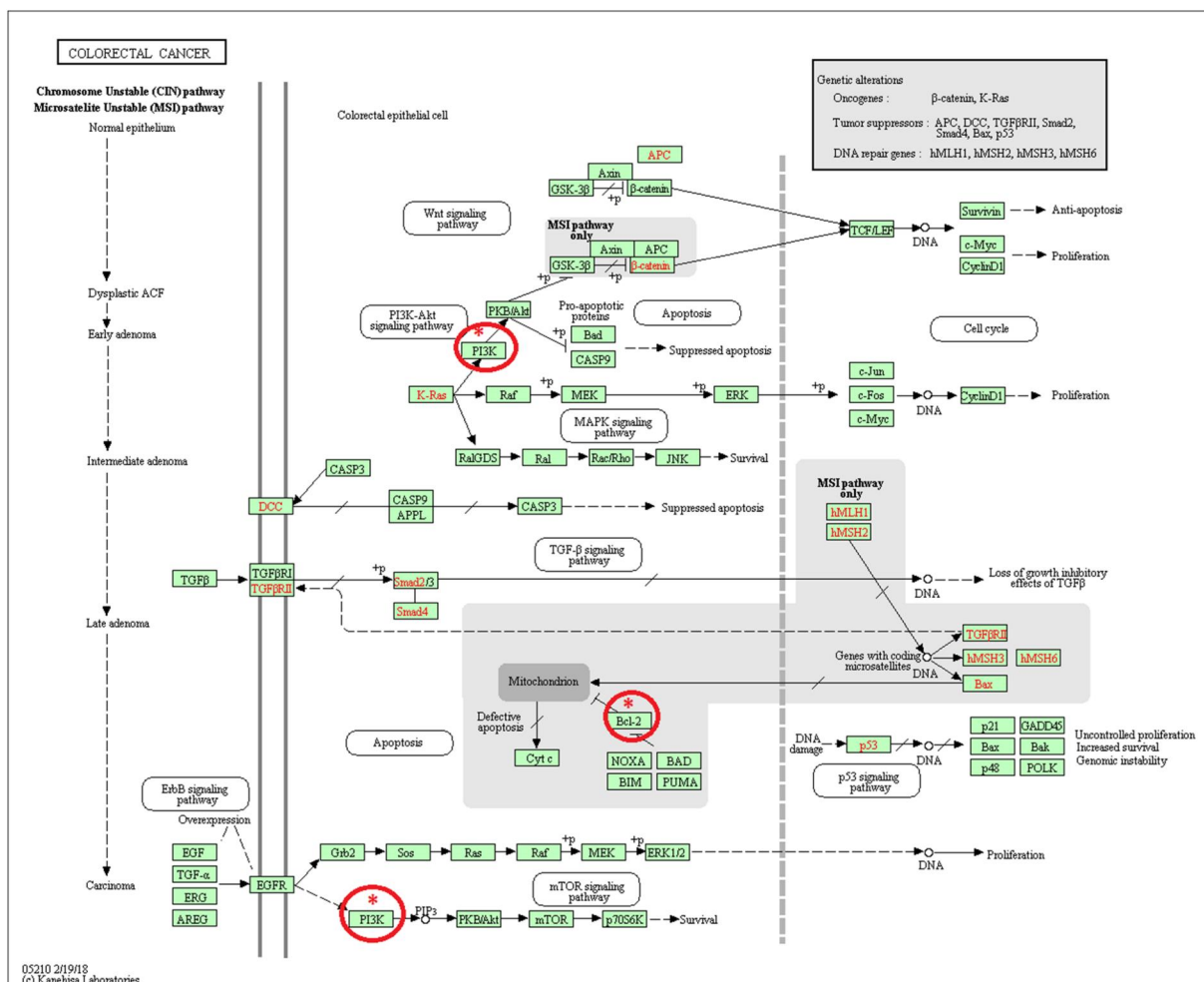


Figure 3. PIK3CA, BCL2, and PIK3CG genes are associated with the colorectal cancer pathway (red circle with asterisk sign).

(Table 2) with the target protein where two hydrogen bonds were formed with Arg A:124 and Gly A:125 residues in the distance of 2.69 Å and 2.26 Å respectively (Figure 5b).

In this simulation, UA has formed four hydrogen bonds with the protein BCL2, which has two more than the

co-crystallised ligand. However, the interaction energy of UA and BCL2 is inferior to that of a co-crystallised complex. This might be due to less interaction between UA and the protein increased survival. Genomic instability

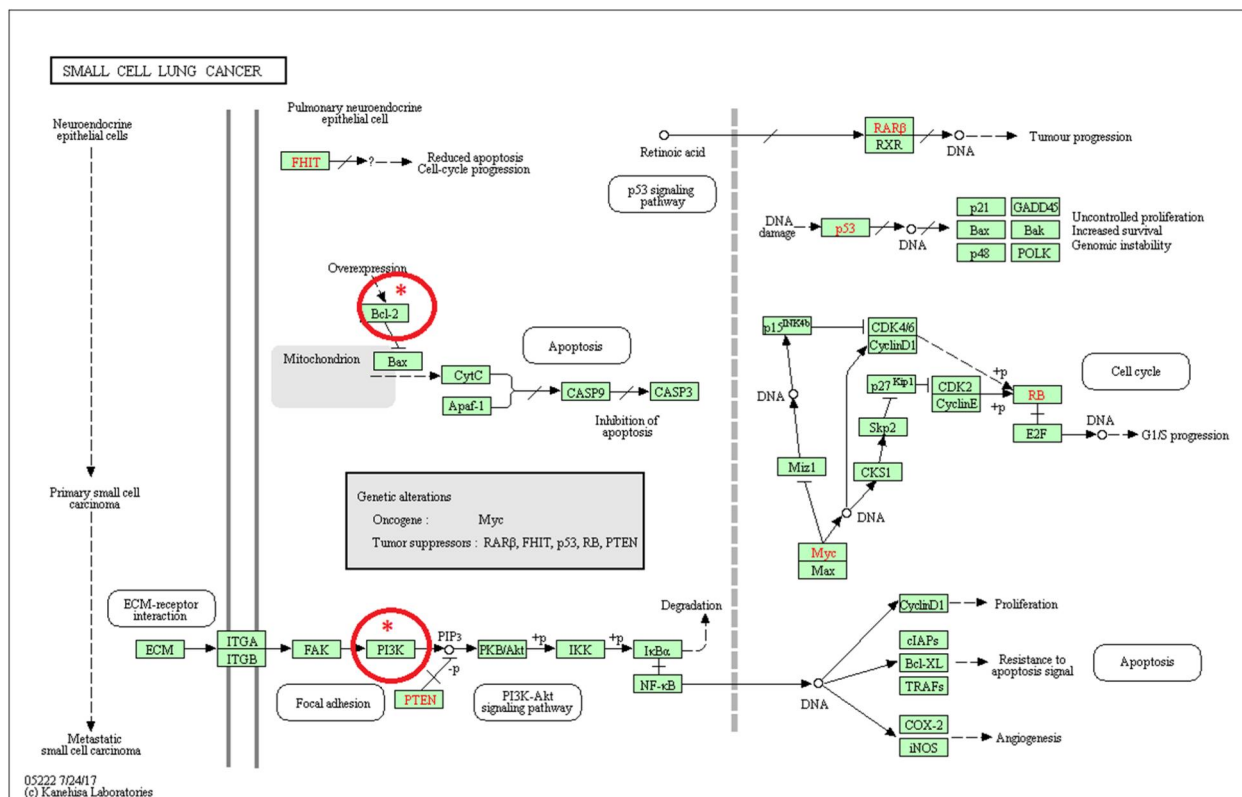


Figure 4. PIK3CA, BCL2, and PIK3CG genes are associated with the small cell lung cancer pathway (red circle with asterisk sign).

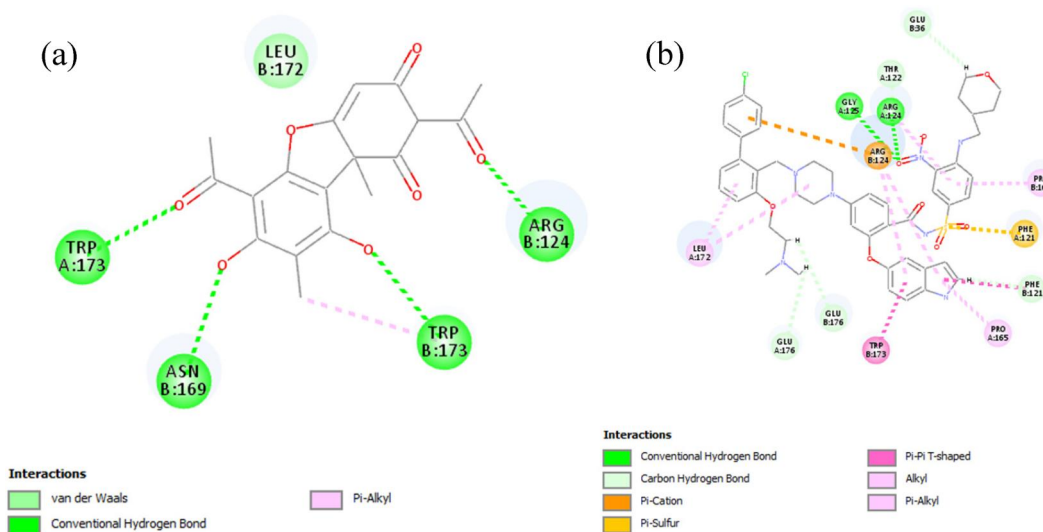


Figure 5. Interaction analysis of (a) UA and; (b) co-crystallised ligand with the target protein of BCL-2 (PDB ID: 4MAN).

Table 2. Molecular docking results of BCL2 with the co-crystallised ligand and UA.

Compound	CDOCKER interaction energy	Number of hydrogen bond	Minimum distance of hydrogen bond	Amino acid residues
UA	-36.5158 kcal/mol	4	2.00 Å	Arg B:124, Asn B:169, Leu B:172, Trp A:173, Trp B:173
Co-crystallised ligand	-73.5126 kcal/mol	2	2.26 Å	Glu B:36, Phe A:121, Phe B:121, Thr A:122, Arg A:124, Arg B:124, Gly A:125, Pro A:165, Pro B:165, Leu A:172, Trp B:173, Glu A:176, Glu B:176

equally essential when coming to the placement in the pocket of protein (Beshnova et al., 2017). Other interactions such as hydrophobic interactions are also accounted for in calculating the binding affinity of the ligand. Since there is a

lack of other interactions between UA and the target protein, it results in weaker interaction energy than it could have been. Besides, the mixing of strong and weaker hydrogen bonds may also lower the binding affinity of the complex

(Chen et al., 2016). Hence, further optimisation of the structure of UA could greatly improve its ability in inhibiting the BCL2 protein.

When interacting with PI3KCA protein, UA demonstrates better fitting than BCL2 (Figure 6a). Two carbonyl group from the UA has mediated two different hydrogen bonds with the amino acid residue LYS A:802 in the distance of 1.86 Å and 2.20 Å, respectively. The oxygen from the furan group in UA also projected a hydrogen bond with the amino acid residue SER A:774 with a distance of 2.35 Å. Besides hydrogen bonding, UA also formed several alkyl bonds with other amino acid residues (Ile A:932, Val A:850, Ile A:848, Ile A:800, Pro A:778 and Met A:772) from the benzene group and methyl group. The binding interaction energy obtained from molecular docking simulation was -44.5995 kcal/mol, which is also a huge difference compared to the co-crystallised ligand. However, as mentioned before, it is possible that structural modification of UA could further enhance the inhibitory effect of UA towards this particular protein for the anticancer treatment of colorectal cancer and small-cell lung cancer.

On the other hand, the co-crystallised ligand (Pubchem CID:124193915) had -67.3009 kcal/mol binding affinity to the target protein with eight hydrogen bonds with Ser A:854, Arg A:770, Val A:851, Asp A:933, Asp A:805, Asp A:810, Lys A:802 and Ser A:774 residues in the distance of 2.63 Å, 1.97 Å, 2.05 Å, 2.83 Å, 2.53 Å, 2.08 Å, 2.11 Å, 2.19 Å, respectively (Table 3 and Figure 6a).

In this simulation, UA had formed three hydrogen bond interactions with the protein, while the co-crystallised ligand had as many as eight hydrogen bonds. Although the co-crystallised ligand forms a much more hydrogen bond with the target protein, the interaction energy between the ligand and target protein is not as much higher than UA as compared to the BCL2 protein. As mentioned before, the optimised hydrogen bond is the requirement of enhancing the binding affinity of the ligand towards a protein, thus, a large number of hydrogen bonds from co-crystallised ligand plays

a negative effect on the binding interaction. Besides, the minimum length of hydrogen bond formed between UA and the residue LYS A:802 is 1.86 Å, which emphasised that this hydrogen bond formation is more optimised than a co-crystallised ligand. From this observation, it is suggested that UA is docking into the target protein with a niche position; because of this, UA can form the optimised hydrogen bond with the amino acid residue. Other than that, the more miniature the length of the hydrogen bond can cause an increase in interaction energy between the ligand and protein (Jiang & Lai, 2002).

The UA compound took on an expanded shape that fit precisely into the binding pockets of the target protein. One hydroxyl hydrogen of the benzene ring projected two hydrogen bonds with the residues of Asp A:964 and Lys A:833 in the distance of 2.20 Å and 1.99 Å, respectively. The methyl group of UA formed two alkyl/pi-alkyl interactions with the residues Pro A:810 and Met A:804. Several other alkyl/pi-alkyl interactions are formed from the interaction of the benzene ring of UA with amino acid residues Ile A:879, Ile A:963 and Ile A:831. The study revealed that UA had -41.9351 kcal/mol binding affinity with the target protein, which is less of a difference to the co-crystallised ligand as compared to BCL2 and PI3KCA proteins. This indicates that UA might have great inhibitory activity against the target protein (PI3KCG) and the structurally modified derivatives could be valuable drug candidates against colorectal cancer as well as small cell lung cancer by targeting PI3KCG protein (Table 4 and Figure 7a).

Meanwhile, the co-crystallised ligand (Puchem CID:53327269) had -50.8015 kcal/mol binding affinity to the target protein with three hydrogen bonds with amino acid residues with their distance Lys A:802 (2.28 Å), Val A:882 (2.01 Å and 2.05 Å) and Lys A:833 (2.55 Å and 2.76 Å).

While in this simulation, the interaction energy of the UA with the target protein is proximate to the co-crystallised ligand. However, the co-crystallised ligand has a slight advantage of having more and better-optimised hydrogen bonds

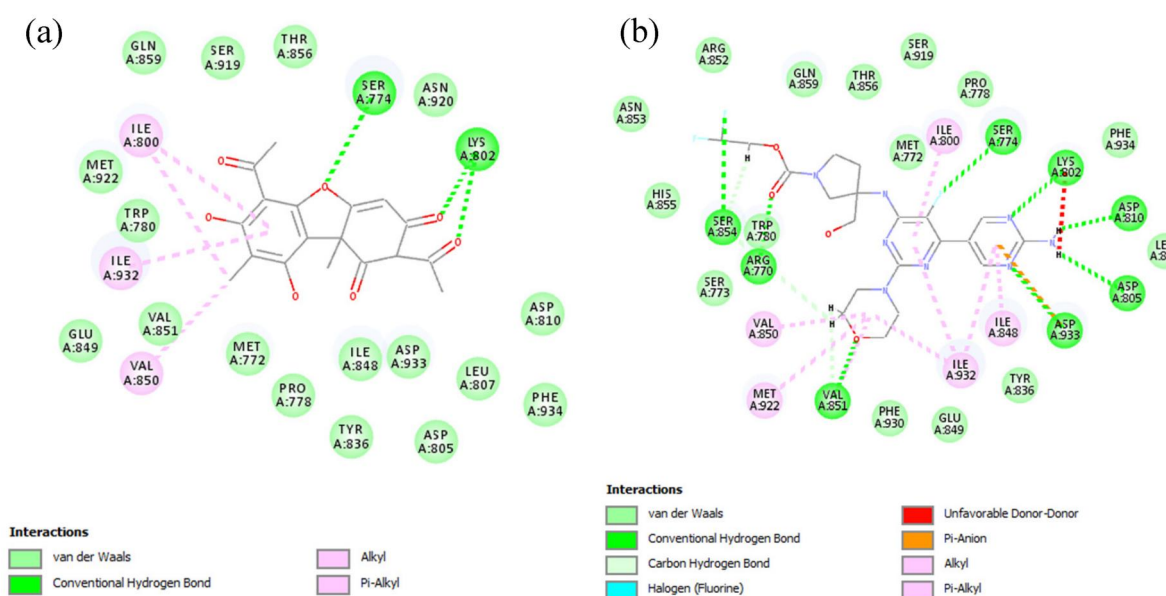


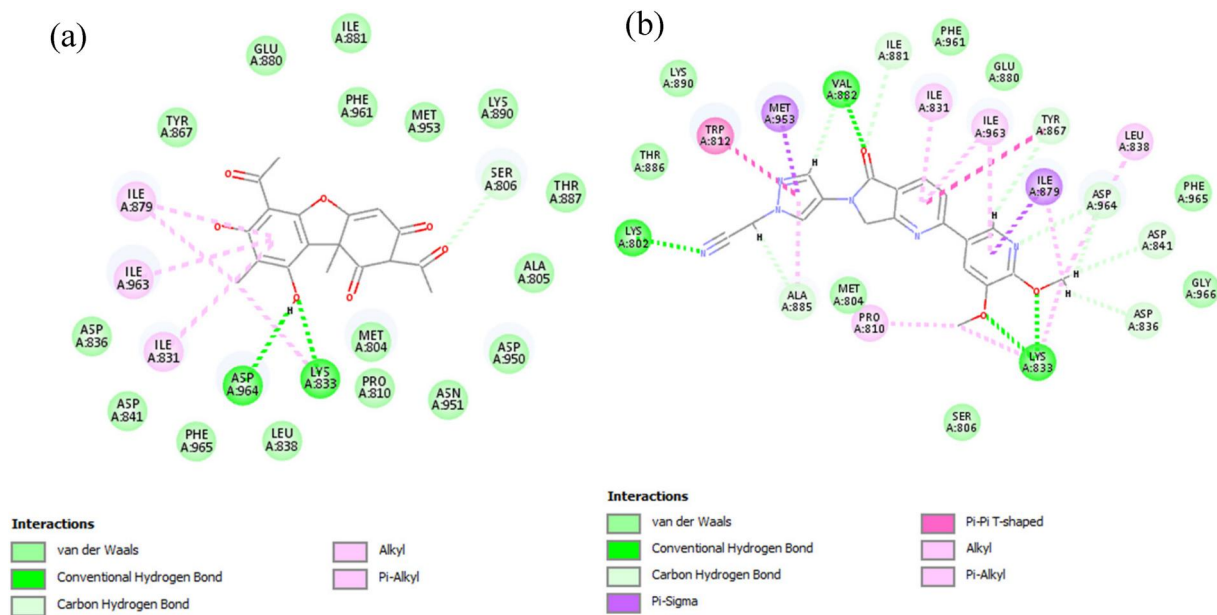
Figure 6. Interaction Analysis of (a) UA and; (b) co-crystallised ligand with the target protein of PI3KCA (PDB ID: 7K6M).

Table 3. Molecular docking results of PI3KCA protein with the co-crystallised ligand and UA.

Compound	CDOCKER interaction energy	Number of hydrogen bond	Minimum distance of hydrogen bond	Amino acid residues
UA	-44.5995 kcal/mol	3	1.86 Å	Ser A:774, Lys A:802, Ile A:932, Val A:850, Ile A:848, Ile A:800, Pro A:778, Met A:772
Co-crystallised ligand	-67.3009 kcal/mol	8	1.97 Å	Ser A:854, Arg A:770, Val A:851, Asp A:933, Asp A:805, Asp A:810, Lys A:802, Ser A:774, Trp A:780, Val A:850, Met A:922, Ile A:932, Ile A:848, Ile A:800

Table 4. Molecular docking results of PI3KCG with the co-crystallised ligand and UA.

Compound	CDOCKER interaction energy	Number of hydrogen bond	Minimum distance of hydrogen bond	Amino acid residues
UA	-41.9351 kcal/mol	2	1.99 Å	Lys A: 833, Asp A:964, Ile A:879, Ile A:963, Ile A:831, Pro A:810, Met A:804, Ser A:806
Co-crystallised ligand	-50.8015 kcal/mol	4	2.01	Lys A:802, Val A:882, Lys A:833, Trp A:812, Ile A:831, Ile A:963, Ala A:885, Ile A:881, Tyr A:867, Asp A:964, Asp A:841, Asp A:836, Met A:953, Ile A:879

**Figure 7.** Interaction Analysis of (a) UA and; (b) co-crystallised ligand with the target protein of small cell lung cancer (PI3KCG) (PDB ID: 6C1S).

and other hydrophobic interactions with the target protein. As mentioned before, further modification of UA might make UA much more effective than the co-crystallised ligand, which also leads to being a potential drug candidate.

2.5. Molecular dynamic simulation

While molecular docking simulation is a tool of simulation used to determine the binding affinity of ligands in a protein, molecular dynamic (MD) simulation is the simulation to

simulate the ligand in a protein within a set time with the addition of surrounding water to it.

Using the Molecular Mechanics Poisson-Boltzmann Surface Area (MMPBSA) method, the MD simulation trajectories computed the binding free energies of the proposed molecules and the target proteins (Hou et al., 2011). It is shown that, for any protein-ligand combination, binding energy calculated using the MMPBSA approach can be regarded as more accurate than the Glide score value. Here, the stronger the binding between the ligand chemical and the targeted protein complex, the bigger the negative free energies of binding value (Table 5). The results clearly showed that the combination of

UA and 6C1S protein had a strong binding free energy of -13.65 kcal/mol. The binding free energy of the UA with the 4MAN and 7K6M protein complex, in comparison, was found to be -1.22 kcal/mol and -2.01 kcal/mol. As a result, UA was determined to have a higher binding affinity for the target proteins based on estimates of free binding energy, leading to the conclusion that the suggested molecule, UA had the potential anti-cancer properties against the PI3K and BCL2 proteins.

Based on the evidence shown on the Root Mean Square Deviation (RMSD) plots (Figure 8(a)), the protein is told to be stabilised at around 7.0 \AA after a considerable fluctuation from 7.5 \AA to 12 \AA , indicating that that protein is undergoing conformational changes during the simulation. However, the stabilisation towards the end of the simulation shows that the protein overall is stable. On the same plots, the RMSD of the ligand in the ligand-protein complex indicates that the ligand is following the conformational changes of the backbone from the protein, which provides information about where the protein is showing its binding activity within the binding site of the protein.

On the Root Mean Square Fluctuation (RMSF) plot shown in Figure 8(b), it is shown that the fluctuations of the amino acid residues are between 1 \AA to 8 \AA . Besides, the N and C terminals are generally having higher fluctuation than any other rigid structures like alpha helices and beta strands in the protein. This indicates that the N and C terminals of the structures are constantly changing within the protein structure. Similarly, the RMSF plot of the ligand (Figure 8(c)) showed that the RMSF of the ligand residues is between $6-7 \text{ \AA}$, indicating that the whole ligand frequently fluctuates within the simulation.

Other than that, the protein-ligand contacts shown in the histogram (Figure 8(d)) reveal that the ligand has multiple interactions with the protein, with the majority forming water bridges. Water bridges are generally hydrogen bonds, with slightly less strictly attached than hydrogen bonds. However, the strength of water bridges is comparable with conventional hydrogen bonds (Utas et al., 2006). Other than that, it also forms multiple hydrogen bonding within the binding pocket, indicating that the ligand is generally very stable within the protein's binding pocket.

Consecutively, the protein-ligand contact plots (Figure 8(e)) show the nature of protein and ligand within the MD simulations. At the same time, the top plot indicates the major interaction between ligand and protein that would result in the stability of interaction, such as hydrophobic interactions and water bridges occurring over the simulation. The trajectory is stabilised throughout the 100 ns while peaking at 45 ns, revealing that the protein and ligand have significant interactions throughout the 100 ns of simulations.

While the bottom panel shows the residues of protein that are responsible for the interaction with the ligand. The amino acid residue Arg A:124, Arg B:124 and Asn B:169 are the most active sites that are in tally with our docking simulation result. Besides that, Figure 8(f) also showed that the ligand has a hydrogen bonding with Arg A:124 and hydrophobic interactions with the residue Pro B:120, Phe A:121 and Pro A:120 more than 30% of the simulation trajectory.

Besides the BCL2 protein, MD simulations on the PI3KCG protein were also run, which is demonstrated in Figure 9. The RMSD of the protein (Figure 9(a)) is pretty much stable and similar to the one of BCL2. However, the RMSD plot of ligand (Figure 9(a)) showed a significant variant with the protein RMSD, where the plot went up to 20 \AA . This result reveals that the distance of ligand travels away from the backbone of the protein is significant, indicating that the ligand is very likely to be diffused away from the binding pocket of the protein starting from 35 ns. Thus, this plot has given us information that the ligand might not be stable in the binding pocket of the protein, leading to the diffusion of the ligand away from the protein.

Figure 9(b) is the RMSF plot for protein PI3KCA; it shows that the fluctuation of the amino acid residue index is between 0.6 \AA to 6 \AA . Similar to the previous proteins, the N and C terminals generally have higher fluctuation than any other rigid structure like alpha helices and beta strands in the protein. Nevertheless, when it comes to the RMSF plot of the ligand (Figure 9(c)) showed significant fluctuation ($5-10 \text{ \AA}$) throughout the whole simulation for the whole ligand, which indicates that the ligand does not sit well within the binding pocket of the protein, while the simulation is going on.

Meanwhile, the protein-ligand contacts histogram (Figure 9(d)) reveals that UA and protein have water bridges and hydrogen bonds as the majority of interactions. Water bridges and hydrogen bonds showed a dominant fraction of the interaction between ligands and proteins. Even though these two interactions dominate the simulations' interactions, they do not have high uptime during the whole simulations occurred. This might explain why the ligand is not sitting within the protein's binding pocket consistently.

Carrying on with the plots (Figure 9(e)) the total contacts between the protein and ligand are stabilised on 5 interactions at the 100 ns time while peaking on the initial trajectory, specifying that the ligand is drifting away from the protein, thus lowering down the interaction number. At the same time, the bottom plot reveals that the amino acid residue Arg A:770 is the only protein that showed a consistent ligand interaction throughout the simulations. The other amino acid residues did form some interactions with the ligand. However, they are not consistent enough to maintain the interaction with the ligand throughout the whole simulations, indicating that the ligand might be rotating within the binding pocket of protein while Arg A:770 served as the centre of rotation. In addition, Figure 9(f) also reveals that only Arg A:770 and Lys A:802 are having significant interaction with the ligand while the rest of the residues do not seem to have interaction exceeding 30% of the time. Nevertheless, compared with the docking simulation results,

Table 5. MM/PBSA calculation by Maestro application of Schrodinger package software.

Protein	PDB ID	Compound	MM/PBSA DG Bind Score (kcal/mol)
BCL2	4MAN	UA	-1.22
PI3KCA	7K6M	UA	-2.01
PI3KCG	6C1S	UA	-13.65

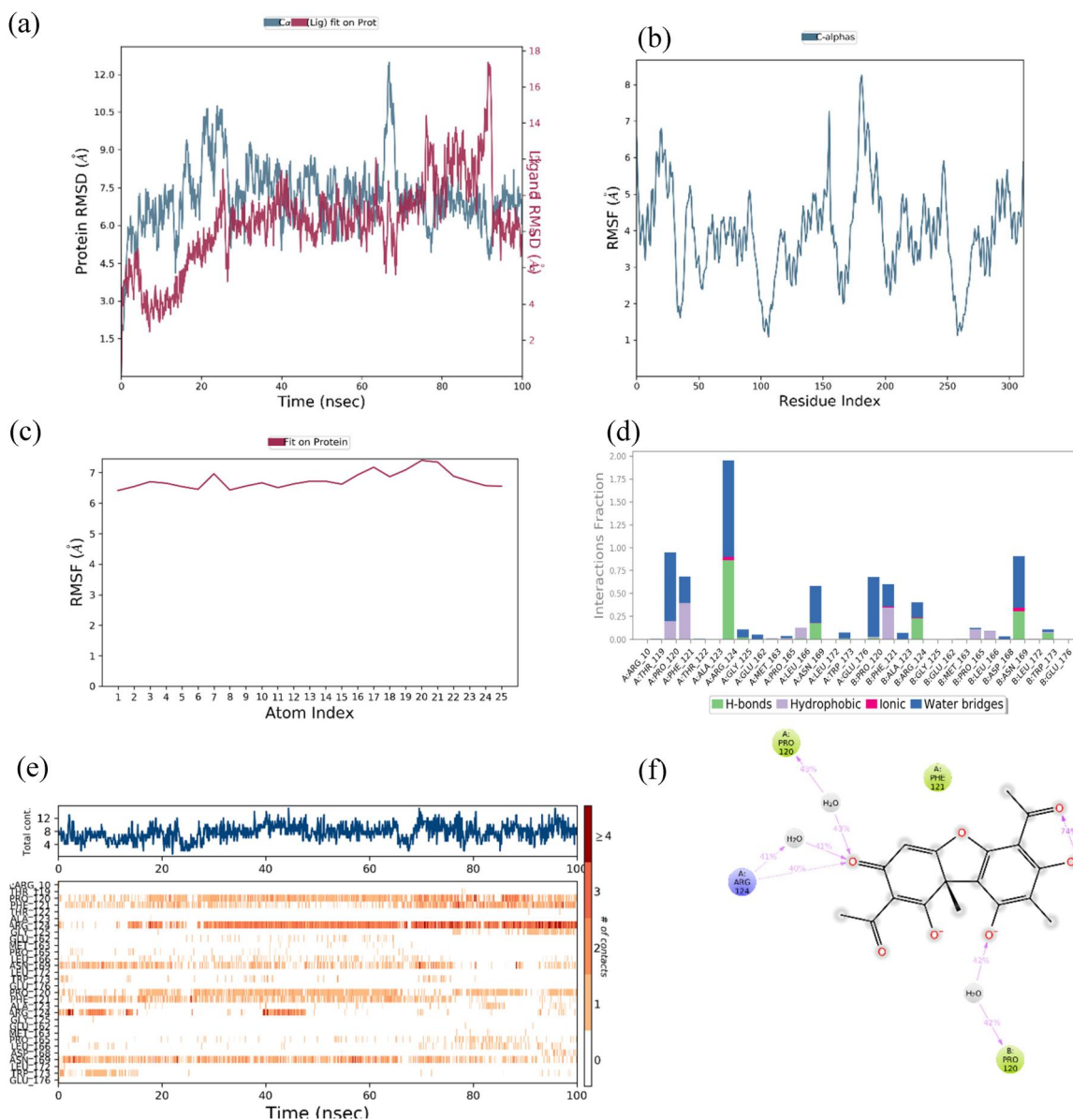


Figure 8. The stability results from BCL2-UA complex by MD simulations at 100 ns trajectory (a) Protein and Ligand RMSD (Å) with time frame over 100 ns; (b) Protein RMSF (Å) plot of protein structural variation from the backbone over the trajectory of 100 ns; (c) Ligand RMSF (Å) plot of 2D ligand structure fluctuation with respect to protein over the trajectory of 100 ns; (d) Histogram showing the proportion of protein-ligand interactions; (e) Protein-ligand contacts; top panel shows total contacts throughout the trajectory of 100 ns; the bottom panel shows the corresponding amino acid residue responsible for the number of interaction with orange colour scale on left; (f) A schematic of detailed ligand atom interactions that occur more than 30.0% of the simulation with the amino acid residues. Purple amino acid residues form charged (negative) interactions with ligands; Green forms hydrophobic interactions.

only the amino acid residue Lys A:802 seems to be tallying with the findings. This variation indicates that UA could not serve as a consistent inhibitor of PI3KCA protein.

While the results of the PI3KCA complex seem to excel in molecular docking simulation, it fails to persist in MD simulation. This is an example of why experimentation results often seem off from what was simulated by using computers. The reason for this case is the addition of surrounding water while the simulation is running, causing much more variable changes to happen in the simulation. Thus, it is concluded that UA is not suitable for use as an inhibitor for PI3KCA protein unless further optimisation of its structure could improve its ability to stay niche within the binding pocket of the protein.

Another variation of PI3K protein, PI3KCG is also being tested with MD simulation (Figure 9). Similarly, according to the RMSD plot (Figure 10(a)), the protein is stabilised around 2.8 Å, indicating that the protein is generally stable throughout the simulation since the fluctuation does not exceed 1–3 Å. Unlike the previous simulation, the ligand RMSD plot of this simulation is stabilised onto 3 Å after a fluctuation at 65 ns. Since the fluctuation of the ligand is not significantly higher than that of the protein, it could be concluded that the ligand is stabilised within the protein's binding pocket.

The RMSF plot shown in Figure 10(b) shows that the fluctuations of the amino acid residues are between 0.6 Å to 4.8 Å. Fluctuation in the plot is similar to the previous two simulations, where N and C terminals generally have higher

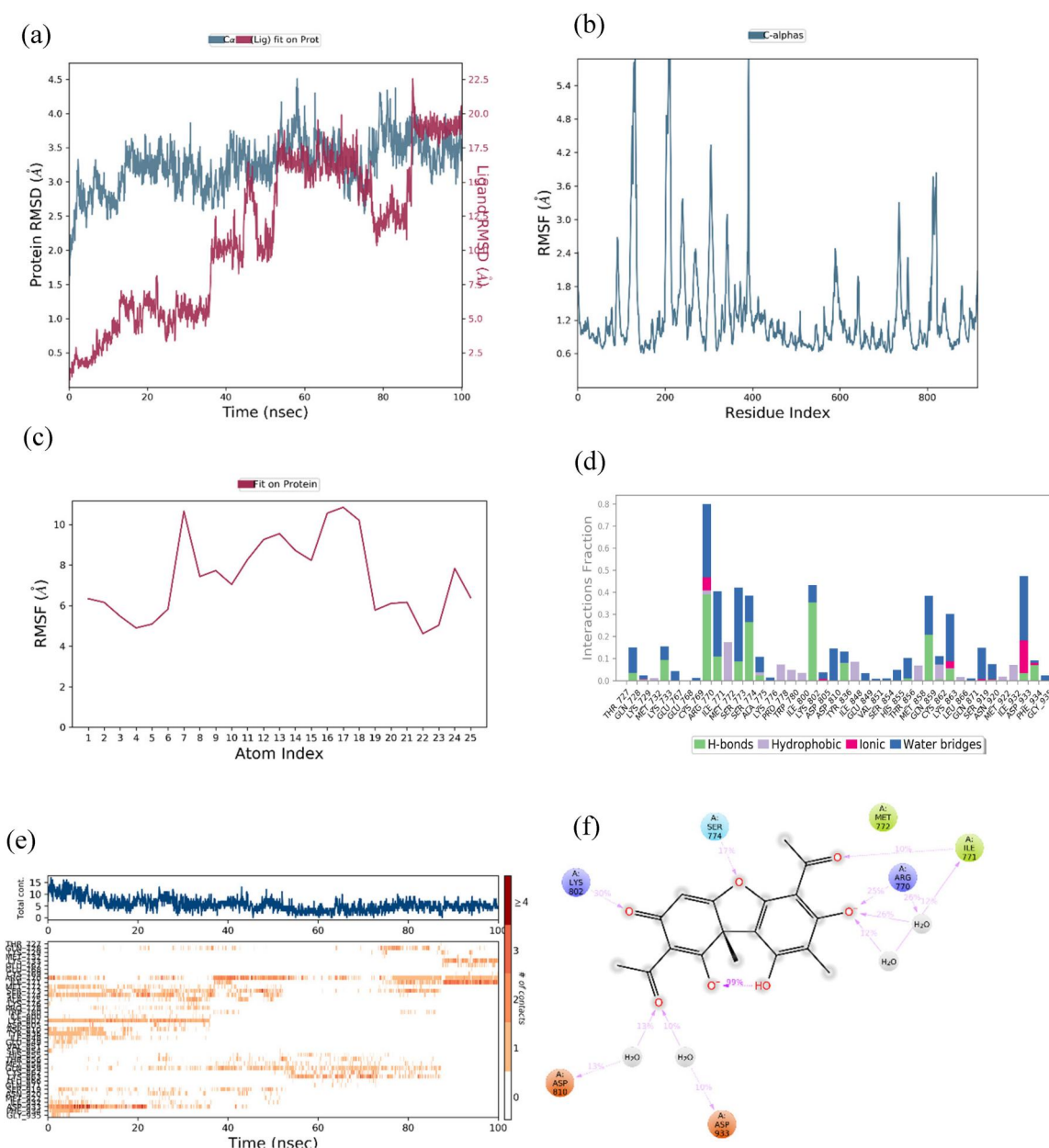


Figure 9. The stability results from PI3KCA complex by MD simulations at 100 ns trajectory (a) Protein and Ligand RMSD (Å) with time frame over 100 ns; (b) Protein RMSF (Å) plot of protein structural variation from the backbone over the trajectory of 100 ns; (c) Ligand RMSF (Å) plot of 2D ligand structure fluctuation with respect to protein over the trajectory of 100 ns; (d) Histogram showing the proportion of protein-ligand interactions; (e) Protein-ligand contacts; top panel shows total contacts throughout the trajectory of 100 ns; the bottom panel shows the corresponding amino acid residue responsible for the number of interaction with orange colour scale on left; (f) A schematic of detailed ligand atom interactions that occur more than 30.0% of the simulation with the amino acid residues. Purple amino acid residues form charged (negative) interactions with ligands; Orange residues form charged (positive) interactions; Green residues form hydrophobic interactions; Blue residues form polar interactions.

fluctuation than any other rigid. Similarly, the RMSF plot of the ligand (Figure 10(c)) showed that the RMSF of the ligand residue is between 1-3 Å, indicating that this ligand does not oscillate much within the binding pocket of protein during the simulations.

Besides that, the protein-ligand contacts histogram (Figure 10(d)) also reveals that UA and protein have multiple interactions such as water bridges, ionic bonds and hydrogen bonds as the majority of interactions. Unlike the previous two simulation results, this protein complex has a significant ionic bond interaction during the simulations, suggesting that the binding affinity of UA could be significant even without much other interaction going on.

Carrying on with the plots (Figure 10(e)), the trajectory is said to be stabilised throughout the 100 ns while peaking at 55 ns, specifying that the protein and ligand have significant interactions throughout the 100 ns of simulations. At the same time, the bottom plot reveals that the amino acid residue Ser A:806, Lys A:808, Lys A:833 and Asp A:964 have interacted with the ligand consistently throughout the 100 ns simulations. Other than that, Asp A:964 is shown to be having the most interaction with the ligand within the 100 ns of simulations. The results shown are also similar to the result obtained from docking simulations. In addition, Figure 10(f) also showed that the UA is having charged interaction with Glu A:880, Asp A:964, Lys A:808 and Lys A:833 with the

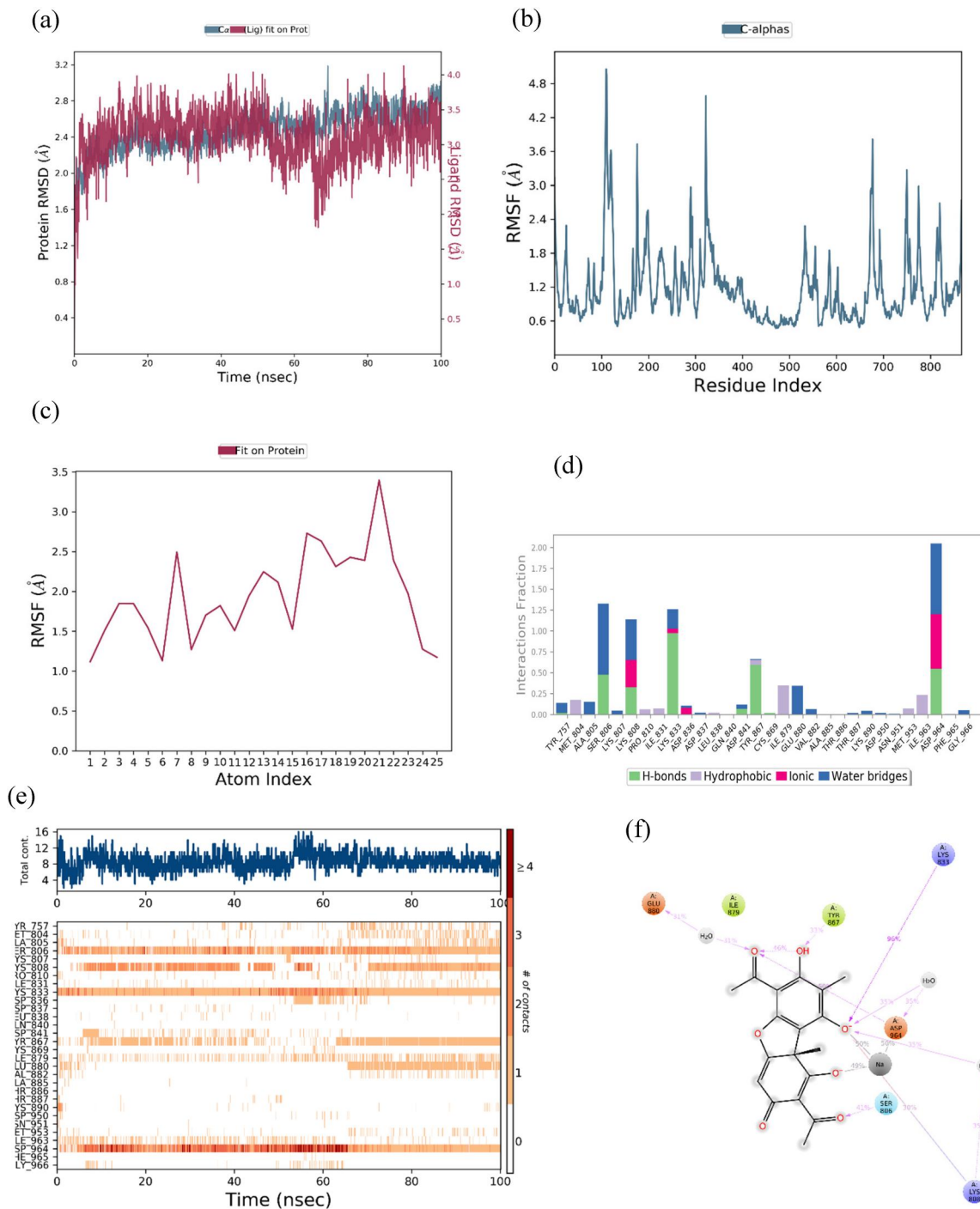


Figure 10. The stability results from PI3KCG complex by MD simulations at 100 ns trajectory (a) Protein and Ligand RMSD (Å) with time frame over 100 ns; (b) Protein RMSF (Å) plot of protein structural variation from the backbone over the trajectory of 100 ns; (c) Ligand RMSF (Å) plot of 2D ligand structure fluctuation with respect to protein over the trajectory of 100 ns; (d) Histogram showing the proportion of protein-ligand interactions; (e) Protein-ligand contacts; top panel shows total contacts throughout the trajectory of 100 ns; the bottom panel shows the corresponding amino acid residue responsible for the number of interaction with orange colour scale on left; (f) A schematic of detailed ligand atom interactions that occur more than 30.0% of the simulation with the amino acid residues. Purple amino acid residues form charged (negative) interactions with ligands; Orange residues form charged (positive) interactions; Green residues form hydrophobic interactions; Blue residues form polar interactions.

protein, while at the same time also forming hydrogen bonds with Ile A:879 and Tyr A:867, and polar coordination with Ser A:806 with protein at more than 30% of the simulation trajectory.

In accordance with this study, the proteins BCL2 and P13KCG, which are associated with the suppression of colorectal and small-cell lung malignancies, represent plausible

promising prospective targets. This discovery might result in the development of novel cancer therapeutic targets.

3. Experimental

The experiment started by building a protein-UA network to determine which protein is the most suitable target of

inhibition for this small molecule. The tools that have been utilised are such as SwissTargetPrediction tools to predict the protein-UA interactions. Cytoscape 3.6.1 to construct the protein-protein interaction network. Kyoto Encyclopedia of Genes and Genomes for the determination of signalling pathways. Then, it is verified by using both molecular docking and MD simulations to further confirm their ability as an inhibitor. All the details steps of the experiment are listed in this section.

3.1. UA–target protein network construction

Succeeding to network pharmacology-based prediction, SwissTargetPrediction tools were also applied to perform a combination of similarity measurements based on known 2D and 3D chemical structures to predict the corresponding potential bioactive targets (probability > 0.1, www.swisstargetprediction.ch) (Gfeller et al., 2014). We downloaded data on compound-gene interactions in people and entered the canonical SMILES structure of all chemicals into target gene identification algorithms. The obtained ligand-protein interaction data of all target proteins were imported into Cytoscape 3.8.2 software to construct a ligand-protein interaction network.

3.2. Construction of protein-protein interaction (PPI) network of the predicted genes

PPI network of the predicted genes was constructed by a search tool for the retrieval of interacting genes (STRING) database (string-db.org/cgi/input.pl; STRING-DB v11.0) (Szkarczyk et al., 2019). The ranking of the target proteins based on the degree of interactions in the PPI network was identified using the Cytoscape plugin cytoHubba (Chin et al., 2014). Data for ligand-protein interaction of all targets were imported into Cytoscape 3.6.1 software to construct a PPI protein interaction network.

3.3. Kyoto encyclopedia of genes and genomes (KEGG) pathway enrichment analyses of the target proteins

To identify the role of target proteins that interact with the active ingredients in gene function and signalling pathways, the Database for Annotation, Visualization and Integrated Discovery (DAVID, david.ncifcrf.gov) v6.8 was employed (Huang da et al., 2009). KEGG (Kanehisa et al., 2017) pathways for significantly associated target proteins with the predicted genes were also identified. The adjusted FDR value ≤ 0.05 , calculated by applying the Benjamini–Hochberg method (Benjamini & Hochberg, 1995), was considered significant.

3.4. Protein preparation for molecular docking

Three-dimensional (3D) structures of BCL2, PI3KCA and PI3KCG macromolecule together with their respective co-crystalise ligands (Pubchem CID:71656179, Pubchem CID:124193915 and Puchem CID:53327269) were retrieved from the literature (Souers et al., 2013; Cheng et al., 2021; Come et al., 2018) and downloaded from the RCSB protein

data bank (PDB). The PDB ID of the macromolecules are 4MAN (BCL2), 7K6M (PI3KCA) and 6C1S (PI3KCG) with the resolution of 2.07 Å, 2.41 Å and 2.31 Å, respectively. The preparation of protein was done using Chimera 1.5.3 and Discovery Studio 3.1. All the hydrogen atoms, missing amino acid residues, and loop segments around the macromolecules' active sites were added, followed by double-checking that various bond arrangements were in the correct order. In addition, all the crystallographic waters were removed from the PDB files.

3.5. Ligand preparation for molecular docking

The structure of UA was retrieved from PubChem (CID: 24211) and constructed using ChemDraw to create a two-dimensional (2D) structure. The built 2D structure of UA was converted to the three-dimensional (3D) format and prepared under the CHARM force field by using Discovery studio 3.1 for docking analysis.

3.6. Molecular docking simulations

The molecular docking simulation was carried out to predict the ligand-protein binding interaction by applying the CDOCKER algorithm using the Discovery Studio 3.1 software for the crystal structure of BCL2, PI3KCA and PI3KCG with UA. Discovery Studio 3.1 with the input PDBQT files of protein was used to create a protein-specific grid box of -28.88 Å, -7.02 Å, -5.96 Å for BCL2, 18.4768 Å, 10.7265 Å, 3.5792 Å for PI3KCA and 21.619 Å, 61.0021 Å, 22.6205 Å for PI3KCG around the active region, with a circle radius of 36.03 Å, 13.3787 Å and 13.1228 Å respectively as well as all other parameters were left as their default values. The Top Hits parameter was set to 10, implying that the top ten conformations of ligand in the protein were saved based on scoring and ranking by the negative value of CDOCKER capacity.

Finally, the molecular interactions were evaluated as well during the docking simulation. Binding energy was calculated in $-kcal/mol$, with the negative value suggesting more significant interactions between the ligand and the target. Two-dimensional and three-dimensional interaction forms of the docked complex were used to observe amino acids present in the ligand-protein binding site using Discovery Studio 3.1 visualiser.

3.7. Molecular dynamic simulation

The selected ligand-protein complex will then be subject to all long atomic range simulation tests for 100 nanoseconds (ns). The whole MD simulation is run by Desmond (Schrödinger Maestro-Desmond Interoperability Tools) (Bhowmick et al., 2020). The "System Builder" module of Desmond was used to create the protein-ligand systems and docked complex. For optimising each BCL2, PI3KCA and PI3KCG bound ligand complex, the OPLS 2005 (optimal potentials for liquid simulations 2005) molecular mechanics force field parameters were assigned (Bharadwaj et al., 2019). The system was dissolved using the TIP3P water model's transferable intermolecular

potential (Huq et al., 2019) and neutralised by changing the appropriate number of counterions. The water box system was built in a cubic form with a space of 10 Å between the water box wall and the protein complex to avoid any overlapping of the system. Desmond's default settings were used to decrease the protein-ligand complex system, with a maximum of 1000 iterations steps utilising the steepest descent (SD) and limited memory Broyden–Fletcher Goldfarb–Shanno (LBFGS) algorithms (Bhowmick et al., 2020). A Coulombic cut-off of 9 Å was utilised for non-bonded or short-range interactions. At the same time, a 10^{-8} tolerance was set for electrostatic interactions using the Particle Mesh Ewald (PME) technique (Cerutti et al., 2009). Moreover, boundary effects were prevented with the use of a periodic boundary condition (PBC) during simulations (Riihimäki et al., 2006). All systems were considerably adjusted before the generation of the MD simulation, with the default protocol being used the majority of the time. An all-atom MD simulation run was submitted for 100 ns in an equilibrated system of NPT (N $1/4$ number of particles, P $1/4$ system pressure, T $1/4$ temperature) ensemble using the Nose–Hoover thermostat (Bhowmick et al., 2020) temperature of 300 K and Martyna–Tobias–Klein barostat (Chelli et al., 2007) bar pressure of 1.0. Roughly 2000 trajectory frames were collected at every 50 picoseconds (ps) interval for the simulation events. The energy of the simulated system was captured every 1.2 ps time. After the MD simulations were completed, the "Simulation Interactions Diagram" module (Anand et al., 2015) embedded in the Desmond programme was used to retrieve simulation-generated information on RMSD, RMSF and protein secondary structure elements. The ligand binding free energies and ligand strain energies can be calculated using MMPBSA for a collection of ligands and a single receptor (Riaz et al., 2022). Following the binding affinity analysis, the MMPBSA was performed using the Desmond Schrodinger suite (Ongaro et al., 2021). We have looked at the differences between the relative binding free affinities of UA with the 6C1S, 7K6M and 4MAN proteins.

4. Conclusion

In summary, the UA anticancer activities mechanism of action was studied through network pharmacology, molecular docking and molecular dynamic simulation. Using KEGG enrichment pathways, the 13 proteins from the PPI analysis that have a significant correlation with UA have been narrowed to the three proteins that UA is most likely to inhibit: BCL2, PI3KCG, and PI3KCA. Among those three proteins, UA displayed a moderate binding affinity with PI3KCG and BCL2 while UA was found to have a weak binding affinity towards B13KCA as demonstrated in molecular docking studies. Despite moderate binding affinity shown by UA, the good stability predicted by MD simulation suggests that UA had a promising potential for inhibiting PI3KCG and BCL2 proteins which are associated with colorectal and small-cell lung cancers. Finally, to fully understand the potential of UA as an anti-cancer medication candidate, further in vivo and in vitro studies should be conducted targeting PI3CG and BCL2 proteins.

Acknowledgements

The authors would like to thank the Ministry of Higher Education for providing financial support under the Fundamental Research Grant Scheme (FRGS) No. FRGS/1/2019/STG01/UMP/02/4 (University Reference: RDU1901160) and Universiti Malaysia Pahang (Internal Research Grant RDU1803148 and PGRS210354).

Disclosure statement

The author has no conflict of interest.

Funding

The author(s) reported there is no funding associated with the work featured in this article.

ORCID

Miah Roney  <http://orcid.org/0000-0003-2512-0837>

References

- ACS. (2022). Types of Cancer Treatment [March 2022]. Available from: <https://www.cancer.org/treatment/treatments-and-side-effects/treatment-types.html>
- Anand, S. A. A., Loganathan, C., Saravanan, K., et al. (2015). Comparison of Molecular Docking and Molecular Dynamics Simulations of 1,3-Thiazin-4-One with MDM2 Protein. *International Letters of Chemistry, Physics and Astronomy*, 60, 161–167.
- Asati, V., Mahapatra, D. K., & Bharti, S. K. (2016). PI3K/Akt/mTOR and Ras/Raf/MEK/ERK signaling pathways inhibitors as anticancer agents: Structural and pharmacological perspectives. *European Journal of Medicinal Chemistry*, 109, 314–341. <https://doi.org/10.1016/j.ejmech.2016.01.012>
- Bangalore, P. K., Vagolu, S. K., Bollikanda, R. K., Veeragoni, D. K., Choudante, P. C., Misra, S., Sriram, D., Sridhar, B., & Kantevari, S. (2020). 2020/01/2 Usnic Acid Enaminone-Coupled 1,2,3-Triazoles as Antibacterial and Antitubercular Agents. *Journal of Natural Products*, 83(1), 26–35. 4. <https://doi.org/10.1021/acs.jnatprod.9b00475>
- Belenahalli Shekarappa, S., Kandagalla, & S., Hanumanthappa, M. (2019). 06/01 A network pharmacology approach to investigate the pharmacological effect of curcumin and capsaicin targets in cancer angiogenesis by module-based PPI network analysis. *Journal of Proteins and Proteomics*, 10, 109–120. <https://doi.org/10.1007/s42485-019-00012-y>
- Benjamini, Y., & Hochberg, Y. (1995). Controlling The False Discovery Rate - A Practical And Powerful Approach To Multiple Testing. *J Royal Statist Soc, Series B*, 57, 289–300.
- Beshnova, D. A., Pereira, J., & Lamzin, V. S. (2017). Estimation of the protein-ligand interaction energy for model building and validation. *Acta Crystallographica. Section D, Structural Biology*, 73(Pt 3), 195–202.
- Bharadwaj, S., Lee, K. E., Dwivedi, V. D., et al. (2019). Discovery of Ganoderma lucidum triterpenoids as potential inhibitors against Dengue virus NS2B-NS3 protease. *Scientific Reports*. 9(1), 19059.
- Bhowmick, S., Alissa, S., Wabaidur, S., et al. (2020). Structure-guided screening of chemical database to identify NS3-NS2B inhibitors for effective therapeutic application in dengue infection. *Journal of Molecular Recognition*, 33
- Cerutti, D. S., Duke, R. E., Darden, T. A., & Lybrand, T. P. (2009). Staggered Mesh Ewald: An extension of the Smooth Particle-Mesh Ewald method adding great versatility. *Journal of Chemical Theory and Computation*, 5(9), 2322.
- Chelli, R., Marsili, S., Barducci, A., & Procacci, P. (2007). Numerical verification of the generalized Crooks nonequilibrium work theorem for non-Hamiltonian molecular dynamics simulations. *The Journal of Chemical Physics*, 127(3), 034110.
- Chen, D., Oezguen, N., Urvil, P., Ferguson, C., Dann, S. M., & Savidge, T. C. (2016). Regulation of protein-ligand binding affinity by hydrogen bond pairing. *Science Advances*, 2(3), e1501240.

- Chen, S., Dobrovolsky, V. N., Liu, F., Wu, Y., Zhang, Z., Mei, N., & Guo, L. (2014). The role of autophagy in usnic acid-induced toxicity in hepatic cells. *Toxicological Sciences: An Official Journal of the Society of Toxicology*, 142(1), 33–44. <https://doi.org/10.1093/toxsci/kfu154>
- Cheng, H., Orr, S. T. M., Bailey, S., Brooun, A., Chen, P., Deal, J. G., Deng, Y. L., Edwards, M. P., Gallego, G. M., Grodsky, N., Huang, B., Jalaie, M., Kaiser, S., Kania, R. S., Kephart, S. E., Lafontaine, J., Ornelas, M. A., Pairish, M., Planken, S., ... Kath, J. C. (2021). Structure-Based Drug Design and Synthesis of PI3K α -Selective Inhibitor (PF-06843195). *Journal of Medicinal Chemistry*, 64(1), 644–661.
- Chin, C.-H., Chen, S.-H., Wu, H.-H., et al. (2014). cytoHubba: Identifying hub objects and sub-networks from complex interactome. *BMC Systems Biology*, 8(4), S11.
- Come, J. H., Collier, P. N., Henderson, J. A., Pierce, A. C., Davies, R. J., Le Tiran, A., O'Dowd, H., Bandarage, U. K., Cao, J., Deininger, D., Grey, R., Krueger, E. B., Lowe, D. B., Liang, J., Liao, Y., Messersmith, D., Nanthakumar, S., Sizensky, E., Wang, J., ... Aronov, A. M. (2018). Design and Synthesis of a Novel Series of Orally Bioavailable, CNS-Penetrant, Isoform Selective Phosphoinositide 3-Kinase γ (PI3K γ) Inhibitors with Potential for the Treatment of Multiple Sclerosis (MS). *Journal of Medicinal Chemistry*, 61(12), 5245–5256.
- Crawford, S. D. (2015). Lichens used in traditional medicine. In: Ranković B, editor. *Lichen secondary metabolites: Bioactive properties and pharmaceutical potential*. Springer International Publishing. p. 27–80.
- Gfeller, D., Grosdidier, A., Wirth, M., Daina, A., Michielin, O., & Zoete, V. (2014). SwissTargetPrediction: A web server for target prediction of bioactive small molecules. *Nucleic Acids Research*, 42(Web Server issue), W32–8.
- Hopkins, A. L. (2007). Network pharmacology. *Nature Biotechnology*, 25(10), 1110–1111. <https://doi.org/10.1038/nbt1007-1110>
- Hou, T., Wang, J., Li, Y., & Wang, W. (2011). Assessing the Performance of the MM/PBSA and MM/GBSA Methods. 1. The Accuracy of Binding Free Energy Calculations Based on Molecular Dynamics Simulations. *Journal of Chemical Information and Modeling*, 51(1), 69–82.
- Huang da, W., Sherman, B. T., & Lempicki, R. A. (2009). Bioinformatics enrichment tools: Paths toward the comprehensive functional analysis of large gene lists. *Nucleic Acids Research*, 37(1), 1–13. <https://doi.org/10.1093/nar/gkn923>
- Huang, Z. (2000). Bcl-2 family proteins as targets for anticancer drug design. *Oncogene*, 19(56), 6627–6631. <https://doi.org/10.1038/sj.onc.1204087>
- Huq, A. M., Wai, L. K., Rullah, K., Mohd Aluwī, M. F. F., Stanslas, J., & Jamal, J. A. (2019). Mar Oestrogenic activity of mimosine in MCF-7 breast cancer cell line through the ER α -mediated pathway. *Chemical Biology & Drug Design*, 93(3), 222–231.
- Hussein, R. K., & Elkhair, H. M. (2021). Molecular docking identification for the efficacy of some zinc complexes with chloroquine and hydroxychloroquine against main protease of COVID-19. *Journal of Molecular Structure*, 1231, 129979. <https://doi.org/10.1016/j.molstruc.2021.129979>
- Jiang, LLai., & L., C. H. (2002). O Hydrogen Bonds at Protein-Protein. *The Journal of Biological Chemistry*, 277(40), 37732–37740. – <https://doi.org/10.1074/jbc.M204514200>
- Kamath, P. R., Sunil, D., Ajees, A. A., Pai, K. S. R., & Biswas, S. (2016). N'-(2-(6-bromo-2-oxo-2H-chromen-3-yl)-1H-indol-3-yl)methylene)benzohydrazide as a probable Bcl-2/Bcl-xL inhibitor with apoptotic and anti-metastatic potential. *European Journal of Medicinal Chemistry*, 120, 134–147. <https://doi.org/10.1016/j.ejmech.2016.05.010>
- Kanehisa, M., Furumichi, M., Tanabe, M., Sato, Y., & Morishima, K. (2017). KEGG: New perspectives on genomes, pathways, diseases and drugs. *Nucleic Acids Research*, 45(D1), D353–d361.
- Kostal, J. (2016). Chapter Four - Computational Chemistry in Predictive Toxicology: Status quo et quo vadis?. In: Fishbein JC, Heilman JM, editors. *Advances in Molecular Toxicology*. Vol. 10: Elsevier. p. 139–186.
- Kwong, S. P., & Wang, C. (2020). Review: Usnic acid-induced hepatotoxicity and cell death. *Environmental Toxicology and Pharmacology*, 80, 103493. <https://doi.org/10.1016/j.etap.2020.103493>
- Leibowitz, B., & Yu, J. (2010). Mitochondrial signaling in cell death via the Bcl-2 family. *Cancer Biology & Therapy*, 9(6), 417–422. <https://doi.org/10.4161/cbt.9.6.11392>
- Liu, P., Cheng, H., Roberts, T. M., & Zhao, J. J. (2009). Aug Targeting the phosphoinositide 3-kinase pathway in cancer. *Nature Reviews. Drug Discovery*, 8(8), 627–644. <https://doi.org/10.1038/nrd2926>
- Liu, T., Dong, G., Xu, F., Han, B., Fang, H., Huang, Y., Zhou, Y., Du, L., & Li, M. (2019). Discovery of Turn-On Fluorescent Probes for Detecting Bcl-2 Protein. *Analytical Chemistry*, 91(9), 5722–5728. <https://doi.org/10.1021/acs.analchem.8b05853>
- Nguyen, V.-K., Sichaem, J., Nguyen, H.-H., Nguyen, X. H., Huynh, T.-T.-L., Nguyen, T.-P., Niamnont, N., Mac, D.-H., Pham, D.-D., Chavasiri, W., Nguyen, K.-P.-P., & Duong, T.-H. (2021). Synthesis and cytotoxic evaluation of usnic acid benzylidene derivatives as potential anticancer agents. *Natural Product Research*, 35(7), 1097–1106. 2021/04/03. <https://doi.org/10.1080/14786419.2019.1639176>
- NIH. (2021). What is cancer?: National Cancer Institute; 2021 [updated May 2021; March 2022]. Available from: <https://www.cancer.gov/about-cancer/understanding/what-is-cancer>
- Noorolyai, S., Shajari, N., Baghbani, E., et al. (2019). The relation between PI3K/AKT signalling pathway and cancer. *Gene*, 698, 120–128.
- Ongaro, A., Oselladore, E., Memo, M., Ribaldo, G., & Gianoncelli, A. (2021). Insight into the LFA-1/SARS-CoV-2 Orf7a Complex by Protein-Protein Docking, Molecular Dynamics, and MM-GBSA Calculations. *Journal of Chemical Information and Modeling*, 61(6), 2780–2787.
- Paris, L., & Bazzoni, G. (2008). Dec The protein interaction network of the epithelial junctional complex: A system-level analysis. *Molecular Biology of the Cell*, 19(12), 5409–5421. <https://doi.org/10.1091/mbc.e08-05-0477>
- Prateeksha, Paliya, B. S., Bajpai, R., et al. (2016). The genus Usnea: A potent phytomedicine with multifarious ethnobotany, phytochemistry and pharmacology. *RSC Advances*, 6(26), 21672–21696. <https://doi.org/10.1039/C5RA24205C>
- Riaz, F., Hossain, M. S., Roney, M., et al. (2022). Evaluation of potential bacterial protease inhibitor properties of selected hydroxyquinoline derivatives: An in silico docking and molecular dynamics simulation approach. *Journal of Biomolecular Structure and Dynamics*. 18, 1–14.
- Riihimäki, E.-S., Martínez, J. M., & Kloos, L. (2006). An evaluation of non-periodic boundary condition models in molecular dynamics simulations using prion octapeptides as probes. *Journal of Molecular Structure: THEOCHEM*, 760(1), 91–98.
- Singh, A., Vanga, S. K., Orsat, V., & Raghavan, V. (2018). Application of molecular dynamic simulation to study food proteins: A review. *Critical Reviews in Food Science and Nutrition*, 58(16), 2779–2789. 2018/11/02. <https://doi.org/10.1080/10408398.2017.1341864>
- Souers, A. J., Levenson, J. D., Boghaert, E. R., Ackler, S. L., Catron, N. D., Chen, J., Dayton, B. D., Ding, H., Enschede, S. H., Fairbrother, W. J., Huang, D. C. S., Hymowitz, S. G., Jin, S., Khaw, S. L., Kovar, P. J., Lam, L. T., Lee, J., Maecker, H. L., Marsh, K. C., ... Elmore, S. W. (2013). ABT-199, a potent and selective BCL-2 inhibitor, achieves antitumor activity while sparing platelets. *Nature Medicine*, 19(2), 202–208.
- Szklarczyk, D., Gable, A. L., Lyon, D., Junge, A., Wyder, S., Huerta-Cepas, J., Simonovic, M., Doncheva, N. T., Morris, J. H., Bork, P., Jensen, L. J., & Mering, C. v (2019). STRING v11: Protein-protein association networks with increased coverage, supporting functional discovery in genome-wide experimental datasets. *Nucleic Acids Research*, 47(D1), D607–d613. <https://doi.org/10.1093/nar/gky1131>
- Utas, J. E., Kritikos, M., Sandström, D., & Akermark, B. (2006). Water as a hydrogen bonding bridge between a phenol and imidazole. *Biochimica et Biophysica Acta*, 1757(12), 1592–1596.
- Vogler, M., Dinsdale, D., Dyer, M. J. S., & Cohen, G. M. (2009). Bcl-2 inhibitors: Small molecules with a big impact on cancer therapy. *Cell Death and Differentiation*, 16(3), 360–367. <https://doi.org/10.1038/cdd.2008.137>
- Wei, Y., Yang, J., Kishore Sakharkar, M., Wang, X., Liu, Q., Du, J., & Zhang, J.-J. (2020). 2020/06/02 Evaluating the inhibitory effect of eight compounds from *Daphne papyracea* against the NS3/4A protease of hepatitis C virus. *Natural Product Research*, 34(11), 1607–1610. <https://doi.org/10.1080/14786419.2018.1519825>
- WHO. (2020). The top 10 causes of death: World Health Organisation; [March 2022]. Available from: <https://www.who.int/news-room/factsheets/detail/the-top-10-causes-of-death>
- Wong, F. H., Huang, C. Y., Su, L. J., et al. (2009). Jan Combination of microarray profiling and protein-protein interaction databases delineates the minimal discriminators as a metastasis network for esophageal squamous cell carcinoma. *International Journal of Oncology*, 34(1), 117–128.